J. Fluid Mech. (2004), *vol.* 511, *pp.* 179–199. © 2004 Cambridge University Press
DOI: 10.1017/S0022112004009565 Printed in the United Kingdom

On the relation between the viscous and inviscid absolute instabilities of the rotating-disk boundary layer

By J. J. HEALEY

Department of Mathematics, Keele University, Keele, Staffs ST5 5BG, UK
j.j.healey@keele.ac.uk

(Received 6 June 2003 and in revised form 5 January 2004)

In this paper we consider the stability of the flow produced by an infinite rotating disk. A large-Reynolds-number asymptotic theory is developed to obtain the non-parallel correction to the local absolute instability (AI) found for this flow by Lingwood (1995), who used the parallel-flow approximation. Our asymptotic theory is based on the inviscid AI underlying the viscous AI and so is expected to give the non-parallel correction to the upper branch of Lingwood's neutral curve for the AI. It is found that non-parallel terms have a destabilizing effect on the AI. Also, it is shown that, although the position of the neutral curve for convective instability is known to depend on choice of measurement quantity, for AI it does not. However, in relating the asymptotic non-parallel results to the numerical parallel results at large Reynolds numbers, it is found that Lingwood's viscous AI does not, after all, asymptote towards the inviscid results. Instead, Lingwood's family of branch points is distinct from a second family of branch points that do asymptote towards the inviscid limit. We show that these two families of branch points are related by a 'super branch point' at which three spatial branches connect simultaneously. Lingwood's branch points, in fact, have a viscous long-wave origin, and will therefore be subjected to non-parallel effects that are some power of the Reynolds number larger than if they had been of inviscid origin.

1. Introduction

Linearized disturbances to spatially developing basic flows are described by sets of partial differential equations, which can be relatively challenging to solve numerically. This is especially true if, for example, the local flow characteristics display absolute instability since then waves grow in both upstream and downstream directions, and this behaviour then raises concerns over the nature of the upstream influence of the downstream boundary conditions. The problem with which we concern ourselves here, the flow produced by an infinite rotating disk, falls into this category.

However, in many spatially developing shear layers of practical interest, this spatial development, which is a consequence of viscous diffusion, is weak, because the Reynolds number, Re, is large. The effect of non-parallel terms, i.e. those in the linearized disturbance equations that contain derivatives with respect to the streamwise coordinate, on disturbance stability will be similarly weak for disturbances with wavelengths comparable to the shear layer thickness, for example inviscidly unstable disturbances. For such disturbances, the viscous terms, i.e. the second-order spatial derivatives, and non-parallel terms are apparently of the same order

https://doi.org/10.1017/S0022112004009565 Published online by Cambridge University Press

of magnitude, but in fact the viscous terms make a greater contribution to the stability characteristics of wall-bounded flows. This is because at large Reynolds numbers their importance is increased in thin viscous wall layers where non-slip boundary conditions apply, and this produces a corresponding increase in their effect on the dispersion relations. Under these circumstances, it is permissible to neglect the non-parallel terms while retaining the viscous terms. This so-called 'parallel-flow approximation' has the great advantage of reducing the disturbance equations from partial differential equations to ordinary differential equations, thus allowing relatively quick numerical solution (provided appropriate methods are used to overcome their considerable stiffness at numerically large Reynolds numbers).

The expediency of the parallel-flow approximation made it important in the historical development of the theory of boundary-layer stability, and means it is still widely used. However, the case for justifying its use is not always as straightforward as indicated in the preceeding paragraph, and the question of determining the quantitative, or qualitative, effect of the non-parallel terms remains important when detailed comparisons with experiment are to be made. Non-Parallel effects become more important the longer the wavelength of the disturbance. Long waves are often characteristic of disturbances whose instability mechanism is viscous rather than inviscid. If the wavelength becomes large enough, as can occur for example with Görtler vortices, see Hall (1983), the non-parallel terms make a leading-order contribution to the dispersion relation and the parallel-flow approximation cannot be justified at all. Mathematically, this is because long enough waves have wavenumbers small enough to cause the terms they multiply in the stability equations to become comparable in size to the non-parallel terms. Physically, with long enough waves the basic flow changes significantly over a single wavelength causing the separation of scales between evolution of wave and evolution of basic flow to be lost, therefore requiring both to be treated together.

It could be argued that the parallel-flow approximation ought only to be used once the asymptotic large-Reynolds-number structure of disturbances has been established. This would indicate whether the fundamental mechanism is a short-wave inviscid one, or a long-wave viscous one, and thus give the order of magnitude of the non-parallel correction. The parallel-flow approximation can then be used if this correction is smaller than $O(1)$. (Strictly speaking, the magnitude of the non-parallel correction is only known as $Re \to \infty$; at any finite value of the Reynolds number issues of series convergence arise and one cannot be certain that there are not higher-order non-parallel terms that dominate the solution for any specific value of the Reynolds number. Nonetheless, we take a pragmatic approach, and assume that the Reynolds number will be high enough for higher-order terms to be negligible). If required, the stabilizing or destabilizing character of the non-parallel terms can then by obtained by carrying out a perturbation expansion to high enough order in the appropriate fractional inverse power of the Reynolds number, like Smith (1979) did for the Blasius boundary layer.

However, within the last decade increases in computing power have meant that the effect of non-parallel terms can be computed relatively conveniently by parabolizing the disturbance equations, as in Bertolotti, Herbert & Spalart (1992), but this approach could not be justified in absolutely unstable flow, since then waves propagate both upstream and downstream. There are other numerical methods for estimating non-parallel effects that do not depend on parabolization, like that proposed by Gaster (1974), and a similar approach to this problem will be presented for publication in due course. Here, however, we take the analytical approach in order to investigate the

https://doi.org/10.1017/S0022112004009565 Published online by Cambridge University Press

fundamental effects produced by non-parallel terms in the large-Reynolds-number limit on the absolute instability of the rotating-disk boundary layer discovered by Lingwood (1995) using the parallel-flow approximation.

It should be pointed out that there is another, perhaps ultimately more important, question concerning the interplay between spatial inhomogeneity and local absolute instability: that of the existence of global modes, and the properties of any such modes, see for example the reviews by Huerre & Monkewitz (1990) and Huerre (2000). A sufficiently spatially extended region of local absolutely unstable flow is usually required in order to sustain an unstable linear global mode. However, the linear global mode properties, e.g. their temporal growth rates, are based on local stability calculations, often at locations in the complex plane of a spatial coordinate, e.g. Soward & Jones (1983), Monkewitz, Huerre & Chomaz (1993). Therefore, the inclusion of non-parallel corrections to the dispersion relation, and hence to the local absolute instability calculations, allows more accurate linear global modes to be calculated. The same considerations apply to the calculation of nonlinear global modes. For example, the secondary absolute instability found by Pier (2003) of nonlinear global modes in the rotating-disk boundary layer are based on parallel-flow calculations, and while this may not affect the qualitative features of the transition scenario described in that paper, detailed quantitative comparisons with experiments or simulations may yet require local non-parallel corrections to be included in the theory.

The linearized disturbance equations are derived in § 2, and far from the disk's axis of rotation a WKB formulation is adopted for the disturbances to make explicit the separation of scales between wave evolution and basic flow evolution. This results in a weakly non-parallel set of disturbance equations, with the Rayleigh equation appearing at leading order. Lingwood (1995) also showed that there is absolute instability in the inviscid stability problem, and conjectured that it represented the large-Reynolds-number limit of her numerical viscous parallel-flow calculation. This is certainly plausible since the much more studied stationary vortices that appear on the rotating disk are known to have an inviscid origin, see Gregory, Stuart & Walker (1955). The results of a comparison between the inviscid Rayleigh solution and the numerical viscous parallel-flow solution for the boundary of absolute instability is presented up to $Re = 1000$ (Re is defined in § 2) that appears to confirm that the upper branch of the numerical viscous solution is asymptoting towards the inviscid solution. This motivates the development in § 3 of a large-Reynolds-number asymptotic expansion whose leading-order term is the neutral inviscid solution. The coefficients in this expansion, which proceeds in powers of $Re^{-1/2}$, have been computed up to and including terms of $O(Re^{-1})$ so that the effects of the first non-parallel terms on the inviscid absolute instability can be determined.

However, a comparison between the asymptotic and numerical solutions for the neutral curve for absolute instability, presented in § 4, reveals surprisingly poor quantitative agreement. Nonetheless, the comparison led to the discovery of a second family of branch points, which are in good agreement with the asymptotic theory. The relation between the two families of branch points, and the regimes where each represent pinch points are also presented in this section. Conclusions are given in § 5.

2. Problem formulation

An infinite disk rotates at constant angular velocity Ω_* in an otherwise still viscous incompressible fluid of kinematic viscosity ν_* (in this paper all dimensional quantities

https://doi.org/10.1017/S0022112004009565 Published online by Cambridge University Press

have been given an asterisk subscript). Viscous stresses at the disk surface accelerate fluid elements near to the disk into almost circular paths, but there is no radial pressure gradient to counter the centrifugal forces acting on these fluid elements, and so fluid near the disk spirals outwards. The disk thus acts as a centrifugal fan, and the fluid thrown outwards in this way is replaced by an axial flow directed towards the disk surface, see Batchelor (1967).

It was shown by von Kármán (1921) that this basic flow can be described by a similarity solution. Batchelor (1951) showed that this flow is also a limiting case of a family of flows with similarity solutions in which both the disk and the fluid far from the disk rotate with different angular velocities. This family also includes as limiting cases the Bödewadt (1940) layer, where the disk is stationary and the fluid rotates, and the Ekman (1905) layer, where fluid and disk co-rotate at almost the same angular velocity. The similarity structure persists when there is a normal flow through the disk wall, e.g. when there is wall suction, Stuart (1954), or blowing, Kuiken (1971). The methods described in the present paper can be applied directly to all of these flows.

2.1. *Governing equations*

We choose to work in cylindrical coordinates in a frame of reference rotating with the disk. The axial and radial coordinates are z_* and r_* respectively, the azimuthal angle is θ, time is t_* and ρ_* is the density of the fluid. The velocities in the radial, azimuthal and axial directions are u_*, v_* and w_* respectively and the pressure is p_*. The governing equations are therefore

$$\frac{1}{r_*}\frac{\partial (r_* u_*)}{\partial r_*} + \frac{1}{r_*}\frac{\partial v_*}{\partial \theta} + \frac{\partial w_*}{\partial z_*} = 0, \tag{2.1a}$$

$$\mathrm{D}_* u_* - \frac{(v_* + \Omega_* r_*)^2}{r_*} = -\frac{1}{\rho_*}\frac{\partial p_*}{\partial r_*} + \nu_* \left(\mathrm{L}_* u_* - \frac{u_*}{r_*^2} - \frac{2}{r_*^2}\frac{\partial v_*}{\partial \theta} \right), \tag{2.1b}$$

$$\mathrm{D}_* v_* + \frac{u_* v_*}{r_*} + 2\Omega_* u_* = -\frac{1}{\rho_* r_*}\frac{\partial p_*}{\partial \theta} + \nu_* \left(\mathrm{L}_* v_* - \frac{v_*}{r_*^2} + \frac{2}{r_*^2}\frac{\partial u_*}{\partial \theta} \right), \tag{2.1c}$$

$$\mathrm{D}_* w_* = -\frac{1}{\rho_*}\frac{\partial p_*}{\partial z_*} + \nu_* \mathrm{L}_* w_*, \tag{2.1d}$$

where the differential operators are

$$\mathrm{D}_* \equiv \frac{\partial}{\partial t_*} + u_*\frac{\partial}{\partial r_*} + \frac{v_*}{r_*}\frac{\partial}{\partial \theta} + w_*\frac{\partial}{\partial z_*}, \quad \mathrm{L}_* \equiv \frac{1}{r_*}\frac{\partial}{\partial r_*}\left(r_*\frac{\partial}{\partial r_*} \right) + \frac{1}{r_*^2}\frac{\partial^2}{\partial \theta^2} + \frac{\partial^2}{\partial z_*^2}. \tag{2.2a, b}$$

Lengths are scaled by the characteristic viscous length scale, and time by the angular velocity of the disk:

$$r_* = (\nu_*/\Omega_*)^{1/2} r, \quad z_* = (\nu_*/\Omega_*)^{1/2} z, \quad t_* = t/\Omega_*. \tag{2.3a, b, c}$$

Flow variables are separated into an axisymmetric steady basic flow, which respects von Kármán's similarity structure, and a more general unsteady part, whose amplitude is characterized by a small parameter $\delta \ll 1$:

$$u_*(r_*, \theta, z_*, t_*) = r_*\Omega_* U(z) + \delta(\nu_*\Omega_*)^{1/2}\hat{u}(r, \theta, z, t), \tag{2.4a}$$

$$v_*(r_*, \theta, z_*, t_*) = r_*\Omega_* V(z) + \delta(\nu_*\Omega_*)^{1/2}\hat{v}(r, \theta, z, t), \tag{2.4b}$$

$$w_*(r_*, \theta, z_*, t_*) = (\nu_*\Omega_*)^{1/2} W(z) + \delta(\nu_*\Omega_*)^{1/2}\hat{w}(r, \theta, z, t), \tag{2.4c}$$

$$p_*(r_*, \theta, z_*, t_*) = \rho_*\nu_*\Omega_* P(z) + \delta\rho_*\nu_*\Omega_*\hat{p}(r, \theta, z, t). \tag{2.4d}$$

https://doi.org/10.1017/S0022112004009565 Published online by Cambridge University Press

2.2. *Basic flow*

Substituting (2.3) and (2.4) into (2.1) and equating terms of $O(\delta^0)$ gives the basic flow similarity equations

$$2U + W' = 0, \tag{2.5a}$$

$$U^2 + WU' - (V+1)^2 = U'', \tag{2.5b}$$

$$WV' + 2U(V+1) = V'', \tag{2.5c}$$

$$WW' = -P' + W'', \tag{2.5d}$$

to be solved subject to boundary conditions

$$U(0) = V(0) = W(0) = 0, \quad U(\infty) = V(\infty) + 1 = 0. \tag{2.6a,b}$$

Here, and throughout, primes denote (sometimes partial) derivatives with respect to z. The numerical solution of (2.5) subject to (2.6) is relatively straightforward, for example by a shooting method where (2.6*a*) provides three initial conditions, with two more initial conditions $U'(0)$ and $V'(0)$ chosen iteratively until (2.6*b*) has been satisfied at a suitable large finite value of z to within some prescribed accuracy. However, the solutions exhibit an unwanted algebraic growth as z increases which could compromise accuracy of the basic flow solution. Instead, the asymptotic large-z series solution of Benton (1966), based on linearizing around the uniform flow far from the disk, has been used, see Healey (2004) for details of the implementation. The solution found has $U'(0) = 0.510236$, $V'(0) = -0.615922$ and $W(\infty) = -0.884474$.

2.3. *Linearized disturbance equations*

Substituting (2.3) and (2.4) into (2.1) and equating terms of $O(\delta)$ gives the linearized disturbance equations

$$\frac{1}{r}\frac{\partial(r\hat{u})}{\partial r} + \frac{1}{r}\frac{\partial \hat{v}}{\partial \theta} + \frac{\partial \hat{w}}{\partial z} = 0, \tag{2.7a}$$

$$\mathrm{D}\hat{u} + rU'\hat{w} + U\hat{u} - 2(V+1)\hat{v} = -\frac{\partial \hat{p}}{\partial r} + \mathrm{L}\hat{u} - \frac{\hat{u}}{r^2} - \frac{2}{r^2}\frac{\partial \hat{v}}{\partial \theta}, \tag{2.7b}$$

$$\mathrm{D}\hat{v} + rV'\hat{w} + U\hat{v} + 2(V+1)\hat{u} = -\frac{1}{r}\frac{\partial \hat{p}}{\partial \theta} + \mathrm{L}\hat{v} - \frac{\hat{v}}{r^2} + \frac{2}{r^2}\frac{\partial \hat{u}}{\partial \theta}, \tag{2.7c}$$

$$\mathrm{D}\hat{w} + W'\hat{w} = -\frac{\partial \hat{p}}{\partial z} + \mathrm{L}\hat{w}, \tag{2.7d}$$

where

$$\mathrm{D} \equiv \frac{\partial}{\partial t} + rU\frac{\partial}{\partial r} + V\frac{\partial}{\partial \theta} + W\frac{\partial}{\partial z}, \quad \mathrm{L} \equiv \frac{1}{r}\frac{\partial}{\partial r}\left(r\frac{\partial}{\partial r}\right) + \frac{1}{r^2}\frac{\partial^2}{\partial \theta^2} + \frac{\partial^2}{\partial z^2}. \tag{2.8a,b}$$

The coefficients depend on both r and z, but not θ nor t. Therefore, Fourier series can be taken in θ (since the flow field is periodic in θ) and Fourier transforms can be taken in t, but the disturbance equations remain partial differential equations, with variables depending on both r and z. Reduction to ordinary differential equations at leading order is only possible far from the axis of rotation, and this is the limit we shall work in.

Let R_* be the dimensional position of interest on the disk, then a Reynolds number, Re, can be introduced that is the ratio of R_* to the characteristic viscous length scale:

$$Re = R_*\left(\frac{\Omega_*}{\nu_*}\right)^{1/2}. \tag{2.9}$$

https://doi.org/10.1017/S0022112004009565 Published online by Cambridge University Press

(Some studies have defined Re^2 to be the Reynolds number, corresponding to a Reynolds number based on length scale R_* and local disk velocity $R_*\Omega_*$). We now introduce a new radial coordinate, ρ, given by

$$r = Re\,\rho \tag{2.10}$$

where $Re \gg 1$ and $\rho = O(1)$ near the position of interest. If $Re\,\alpha \gg 1$, where α is the radial wavenumber, then the radial wavelength is small compared with the distance to the axis of rotation, and the basic flow does not vary significantly on the length scales associated with the disturbance. This separation between the length scale of disturbance evolution and the length scale of basic flow evolution allows a WKB formulation to be adopted for the disturbance structure, and so we let

$$\hat{u}(r,\theta,z,t) = u(\rho,z)\exp \mathrm{i}Re\left(\int \alpha(\rho)\,\mathrm{d}\rho + \beta\theta - \omega t\right), \tag{2.11a}$$

$$\hat{v}(r,\theta,z,t) = v(\rho,z)\exp \mathrm{i}Re\left(\int \alpha(\rho)\,\mathrm{d}\rho + \beta\theta - \omega t\right), \tag{2.11b}$$

$$\hat{w}(r,\theta,z,t) = w(\rho,z)\exp \mathrm{i}Re\left(\int \alpha(\rho)\,\mathrm{d}\rho + \beta\theta - \omega t\right), \tag{2.11c}$$

$$\hat{p}(r,\theta,z,t) = Re\,p(\rho,z)\exp \mathrm{i}Re\left(\int \alpha(\rho)\,\mathrm{d}\rho + \beta\theta - \omega t\right), \tag{2.11d}$$

where $Re\,\beta$ is an integer and ω is the scaled angular frequency of the wave. We assume $Re\,\beta \gg 1$ and so will neglect the discretization of β, which is the scaled azimuthal wavenumber. Substituting (2.11) into (2.7) gives

$$\mathrm{i}\alpha u + \frac{\mathrm{i}\beta}{\rho}v + w' = -\frac{1}{Re\,\rho}\left[u + \rho\frac{\partial u}{\partial \rho}\right], \tag{2.12a}$$

$$\left(\mathrm{i}\alpha U + \frac{\mathrm{i}\beta}{\rho}V - \frac{\mathrm{i}\omega}{\rho}\right)u + U'w = -\frac{\mathrm{i}\alpha}{\rho}p + \frac{1}{Re\,\rho}\left[u'' - \alpha^2 u - \frac{\beta^2}{\rho^2}u + 2(V+1)v - Uu - Wu' - \rho U\frac{\partial u}{\partial \rho} - \frac{\partial p}{\partial \rho}\right] + O(Re^{-2}), \tag{2.12b}$$

$$\left(\mathrm{i}\alpha U + \frac{\mathrm{i}\beta}{\rho}V - \frac{\mathrm{i}\omega}{\rho}\right)v + V'w = -\frac{\mathrm{i}\beta}{\rho^2}p + \frac{1}{Re\,\rho}\left[v'' - \alpha^2 v - \frac{\beta^2}{\rho^2}v - 2(V+1)u - Uv - Wv' - \rho U\frac{\partial v}{\partial \rho}\right] + O(Re^{-2}), \tag{2.12c}$$

$$\left(\mathrm{i}\alpha U + \frac{\mathrm{i}\beta}{\rho}V - \frac{\mathrm{i}\omega}{\rho}\right)w = -\frac{1}{\rho}p' + \frac{1}{Re\,\rho}\left[w'' - \alpha^2 w - \frac{\beta^2}{\rho^2}w - W'w - Ww' - U\frac{\partial w}{\partial \rho}\right] + O(Re^{-2}), \tag{2.12d}$$

where primes denote partial differentiation with respect to z. The boundary conditions for solving the leading-order inviscid problem are $w(\rho,0) = w(\rho,\infty) = 0$, and for the viscous problem these are supplemented by $u(\rho,0) = v(\rho,0) = u(\rho,\infty) = v(\rho,\infty) = 0$.

The equations (2.12) show that the non-parallel terms, i.e. those involving derivatives with respect to the radial coordinate ρ, are small when Re is large and α, β/ρ and ω/ρ are $O(1)$, i.e. (2.12) are only weakly non-parallel. Under these conditions, the non-parallel terms are of the same order of magnitude as the Coriolis and streamline curvature terms, but, as will be discussed in § 3, the viscous terms have a larger

https://doi.org/10.1017/S0022112004009565 Published online by Cambridge University Press

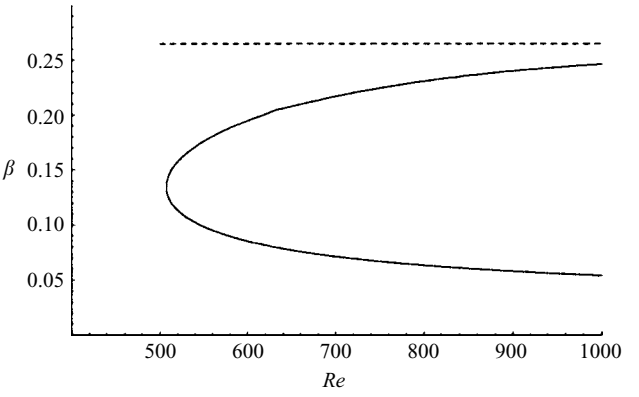


FIGURE 1. Solid line is the neutral curve for absolute instability calculated using the sixth-order parallel-flow approximation; dashed line is the neutral inviscid value (2.13*b*) for absolute instability.

effect on the dispersion relation. Therefore, the non-parallel, Coriolis and streamline curvature terms can be consistently neglected and (2.12) reduced to a fourth-order ordinary differential equation. However, if only the non-parallel terms are neglected (2.12) can be reduced to a sixth-order ordinary differential equation. It is known that the critical Reynolds number for stationary vortices depends sensitively on whether or not the Coriolis and streamline curvature terms are included. In fact, Hall (1986) has shown that Coriolis terms become of the same order as the viscous terms on the long-wave lower branch of the stationary-vortices neutral curve, and this may explain the strong dependence of the stationary-vortices critical Reynolds number on whether or not the Coriolis terms are included. However, Hall's lower-branch analysis also confirms that non-parallel terms are of higher order there too, justifying use of the parallel-flow approximation for all unstable stationary vortices at high enough Reynolds numbers (although the waves are longer near the lower branch, they are not long enough to invalidate the parallel-flow approximation).

There is as yet no corresponding analysis for the long-wave lower branch of the absolute-instability neutral curve, though clearly one would be desirable. Our aim in this paper is to provide an asymptotic analysis of the short-wave upper branch of the absolute-instability neutral curve, and use it to estimate the effect of non-parallel terms on the absolute instability in this part of parameter space.

Lingwood (1995) has shown that in the inviscid limit, i.e. neglecting $O(Re^{-1})$ terms in (2.12), there is an upper limit to β/ρ for the existence of absolute instability. We find that the eigenvalues for the boundary of inviscid absolute instability are

$$\alpha_0 = 0.3383 - 0.0583\mathrm{i}, \quad \beta_0/\rho = 0.2652, \quad \omega_0/\rho = -0.0698. \qquad (2.13a, b, c)$$

These are eigenvalues for which $\partial\omega/\partial\alpha = 0$ in the inviscid limit, for constant β and ρ. It may be verified that this branch point is a pinch point, i.e. it represents a coalescence between an upstream propagating wave and a downstream propagating wave in accordance with the Briggs–Bers criterion for absolute instability, see Briggs (1964). When $0 < \beta/\rho < 0.2652$, the pinch point gives $\mathrm{Im}(\omega/\rho) > 0$, and hence there is absolute instability in this range. Figure 1 shows a comparison between this inviscid neutral absolute-instability result, and the absolute-instability neutral curve obtained by solving numerically the parallel-flow sixth-order ordinary differential equations obtained by setting $\partial/\partial\rho = 0$ and neglecting $O(Re^{-2})$ terms in (2.12). Note that when

https://doi.org/10.1017/S0022112004009565 Published online by Cambridge University Press

comparisons are made with parallel-flow results, local dimensionless variables are used by taking $\rho = 1$. The numerical procedure was based on expanding quantities in terms of Chebyshev polynomials, see Orszag (1971). The critical Reynolds number for absolute instability was found to be $Re = 507.4$ (Lingwood 1997 quotes $Re = 507.3$).

Figure 1 suggests that the upper branch of the parallel-flow branch points asymptotes towards the inviscid value (2.13*b*) as Re increases. Therefore, we take (2.13) as the starting point for the asymptotic large-Reynolds-number theory for the upper branch of the neutral curve for absolute instability.

3. Asymptotic non-parallel branch points

The method of matched asymptotic expansions has been used to obtain solutions to (2.12) as $Re \to \infty$, with leading-order inviscid eigenvalues given by (2.13). This method is used because the disturbance solution has its own boundary-layer structure. At leading order the solution is inviscid and has a finite slip velocity at the wall. When viscosity is included, its dominant role is to enforce the non-slip boundary condition at the wall, and this leads to the existence of a thin viscous layer at the wall. The order of magnitude of the thickness of this layer is found as follows. Let $z = \epsilon Z$, where ϵ represents the thickness of the layer, and the viscous-layer variable $Z = O(1)$ in the viscous layer. The left-hand side of (2.12*a*) shows that in the viscous layer w must be $O(\epsilon)$ smaller than u and v (since $\partial/\partial z = \epsilon^{-1}\partial/\partial Z$). U and V are proportional to z in the viscous layer, and hence are of $O(\epsilon)$ in the viscous layer. Therefore, the dominant inviscid terms in (2.12*b*, *c*) are the unsteady terms, and the pressure is chosen to be of the same order. The thickness of the viscous layer is chosen so that the viscous terms u'' and v'' are of the same order as the dominant inviscid terms in the viscous layer, giving $\epsilon = Re^{-1/2}$. (The corresponding result for stationary vortices, $\epsilon = Re^{-1/3}$, is obtained by repeating the above argument with $\omega = 0$, leading instead to a balance between the viscous terms and the convective terms, as first shown by Hall 1986. The unsteady viscous layer needed here is therefore thinner than the steady viscous layer of stationary vortices).

The presence of a viscous layer of thickness of $O(Re^{-1/2})$ leads to $O(Re^{-1/2})$ corrections to the inviscid dispersion relation. Therefore, let

$$\alpha = \alpha_0 + \epsilon\alpha_1 + \epsilon^2\alpha_2 + \ldots, \tag{3.1a}$$

$$\beta = \beta_0 + \epsilon\beta_1 + \epsilon^2\beta_2 + \ldots, \tag{3.1b}$$

$$\omega = \omega_0 + \epsilon\omega_1 + \epsilon^2\omega_2 + \ldots, \tag{3.1c}$$

where α_0, β_0 and ω_0 are given by (2.13) and $\epsilon = Re^{-1/2}$.

3.1. *Viscous wall layer*

In the viscous layer all variables are expanded in accordance with the scaling arguments presented above. Let

$$u(\rho, z) = U_0(\rho, Z) + \epsilon U_1(\rho, Z) + \ldots, \tag{3.2a}$$

$$v(\rho, z) = V_0(\rho, Z) + \epsilon V_1(\rho, Z) + \ldots, \tag{3.2b}$$

$$w(\rho, z) = \epsilon W_0(\rho, Z) + \epsilon^2 W_1(\rho, Z) + \ldots, \tag{3.2c}$$

$$p(\rho, z) = P_0(\rho, Z) + \epsilon P_1(\rho, Z) + \ldots. \tag{3.2d}$$

In the viscous layer the basic flow takes the form

$$U = \epsilon U'(0)Z + O(\epsilon^2), \quad V = \epsilon V'(0)Z + O(\epsilon^2), \quad W = O(\epsilon^2). \tag{3.3a, b, c}$$

https://doi.org/10.1017/S0022112004009565 Published online by Cambridge University Press

Substituting (3.1), (3.2) and (3.3) into (2.12) and equating the leading-order, and next-order, coefficients of ϵ, gives a set of ordinary differential equations for the variables introduced in (3.2). These equations can be reduced to

$$\frac{\partial^4 W_0}{\partial Z^4} + \mathrm{i}\omega_0 \frac{\partial^2 W_0}{\partial Z^2} = 0, \tag{3.4a}$$

$$\frac{\partial P_0}{\partial Z} = 0, \tag{3.4b}$$

and

$$\frac{\partial^4 W_1}{\partial Z^4} + \mathrm{i}\omega_0 \frac{\partial^2 W_1}{\partial Z^2} = \mathrm{i}\left[\rho\alpha_0 Q_0' Z - \omega_1\right] \frac{\partial^2 W_0}{\partial Z^2}, \tag{3.5a}$$

$$\frac{\partial P_1}{\partial Z} = 0, \tag{3.5b}$$

where

$$Q_0' = Q_0'(\rho) = \frac{\partial Q}{\partial z}(\rho, 0), \quad Q(\rho, z) = U + \frac{\beta_0}{\rho\alpha_0} V. \tag{3.6a, b}$$

The solutions to (3.4) and (3.5) that satisfy the viscous wall boundary conditions

$$W_0(\rho, 0) = \frac{\partial W_0}{\partial Z}(\rho, 0) = W_1(\rho, 0) = \frac{\partial W_1}{\partial Z}(\rho, 0) = 0 \tag{3.7}$$

and that do not grow exponentially in Z are

$$W_0 = A_0(\rho)[\exp(-\sqrt{-\mathrm{i}\omega_0} Z) - 1 + \sqrt{-\mathrm{i}\omega_0} Z], \tag{3.8a}$$

$$P_0 = B_0(\rho), \tag{3.8b}$$

$$W_1 = A_1(\rho)[\exp(-\sqrt{-\mathrm{i}\omega_0} Z) - 1 + \sqrt{-\mathrm{i}\omega_0} Z] + \frac{A_0 Z}{4\omega_0}\{[(\rho\alpha_0 + Q_0' Z - 2\omega_1)\sqrt{-\mathrm{i}\omega_0} + 5\rho\alpha_0 Q_0'] \exp(-\sqrt{-\mathrm{i}\omega_0} Z) + 2\omega_1 \sqrt{-\mathrm{i}\omega_0} - 5\rho\alpha_0 Q_0'\}, \tag{3.8c}$$

$$P_1 = B_1(\rho), \tag{3.8d}$$

where $\sqrt{}$ denotes the root with postive real part.

3.2. *Inviscid region*

The appropriate expansions in the inviscid region are

$$u(\rho, z) = u_0(\rho, z) + \epsilon u_1(\rho, z) + \epsilon^2 u_2(\rho, z) + \ldots, \tag{3.9a}$$

$$v(\rho, z) = v_0(\rho, z) + \epsilon v_1(\rho, z) + \epsilon^2 v_2(\rho, z) + \ldots, \tag{3.9b}$$

$$w(\rho, z) = w_0(\rho, z) + \epsilon w_1(\rho, z) + \epsilon^2 w_2(\rho, z) + \ldots, \tag{3.9c}$$

$$p(\rho, z) = p_0(\rho, z) + \epsilon p_1(\rho, z) + \epsilon^2 p_2(\rho, z) + \ldots. \tag{3.9d}$$

Substituting (3.1) and (3.9) into (2.12) and equating coefficients of ϵ at successive orders leads to ordinary differential equations for all the new variables introduced in (3.9). After some manipulation, the leading-order equations can be reduced to the Rayleigh equation, and the higher-order equations can be reduced to forced Rayleigh equations:

$$w_0'' - \left(\frac{Q''}{Q - c_0} + \gamma_0^2\right) w_0 = 0, \tag{3.10a}$$

$$w_1'' - \left(\frac{Q''}{Q - c_0} + \gamma_0^2\right) w_1 = f_1(z), \tag{3.10b}$$

https://doi.org/10.1017/S0022112004009565 Published online by Cambridge University Press

$$w_2'' - \left(\frac{Q''}{Q-c_0} + \gamma_0^2\right) w_2 = f_2(z), \tag{3.10c}$$

where

$$f_1 = \left\{ 2\left(\alpha_0\alpha_1 + \frac{\beta_0\beta_1}{\rho^2}\right) + \left(\frac{\alpha_1}{\alpha_0} - \frac{\beta_1}{\beta_0}\right)\frac{U''}{Q-c_0} - \left[\left(\frac{\alpha_1}{\alpha_0} - \frac{\beta_1}{\beta_0}\right)U + \frac{c_0\beta_1 - c_1\beta_0}{\beta_0}\right]\frac{Q''}{(Q-c_0)^2}\right\} w_0, \tag{3.11a}$$

$$\gamma_0^2 = \alpha_0^2 + \left(\frac{\beta_0}{\rho}\right)^2, \quad c_0 = \frac{\omega_0}{\rho\alpha_0}, \quad c_1 = \frac{\omega_1}{\rho\alpha_0}. \tag{3.11 b,c,d}$$

and f_2 was obtained using a symbolic manipulation package, and contains too many terms to write out here. Note that f_2 includes the Coriolis and streamline curvature terms and the first non-parallel terms, i.e. those involving partial derivatives with respect to ρ. It also includes the viscous terms; at this order viscous effects are no longer confined to the wall layer, but extend over the whole flow.

The leading-order solution w_0 is obtained by numerically solving (3.10a) using the eigenvalues (2.13) for the neutral inviscid pinch point (for these eigenvalues the critical points, where $Q = c_0$, are arranged in the complex z-plane in such a way that the solution path can be taken along the real z-axis). Equations (3.10b,c) can be solved numerically, but their behaviour for small z is required in order to match to the viscous solutions (3.8). This behaviour can be obtained by expressing the solutions for w_1 and w_2 in terms of w_0. For example,

$$w_1 = w_0 \int_0^z \frac{1}{w_0^2} \int_\infty^t w_0 f_1 \, \mathrm{d}s \, \mathrm{d}t \tag{3.12}$$

satisfies (3.10b) and the outer boundary condition since f_1 is proportional to w_0 for large z by (3.11a). However, instead, we extract the singular part of the integrand and choose

$$w_1 = w_0 \int_0^z \frac{1}{w_0^2} \int_\infty^t w_0 f_1 \, \mathrm{d}s - \frac{1}{(w_0'(\rho,0)t)^2} \int_\infty^0 w_0 f_1 \, \mathrm{d}s \, \mathrm{d}t - \frac{w_0}{w_0'(\rho,0)^2 z} \int_\infty^0 w_0 f_1 \, \mathrm{d}t \tag{3.13}$$

since $w_0''(\rho,0) = 0$ by (3.10a). The behaviour for small z is then quickly found:

$$w_1 \sim \left[2\left(\alpha_0\alpha_1 + \frac{\beta_0\beta_1}{\rho^2}\right) I_{1a} + \left(\frac{\alpha_1}{\alpha_0} - \frac{\beta_1}{\beta_0}\right)(I_{1b} - I_{1c}) - \frac{c_0\beta_1 - c_1\beta_0}{\beta_0} I_{1d} \right] w_0'(\rho,0) + O(z^2), \tag{3.14}$$

where

$$I_{1a} = \frac{1}{w_0'(\rho,0)^2} \int_0^\infty w_0^2 \, \mathrm{d}z, \qquad I_{1b} = \frac{1}{w_0'(\rho,0)^2} \int_0^\infty \frac{U'' w_0^2}{Q-c_0} \, \mathrm{d}z, \tag{3.15a,b}$$

$$I_{1c} = \frac{1}{w_0'(\rho,0)^2} \int_0^\infty \frac{U Q'' w_0^2}{(Q-c_0)^2} \, \mathrm{d}z, \quad I_{1d} = \frac{1}{w_0'(\rho,0)^2} \int_0^\infty \frac{Q'' w_0^2}{(Q-c_0)^2} \, \mathrm{d}z. \tag{3.15c,d}$$

When evaluated using (2.13) these integrals take the values $I_{1a} = 1.564 + 0.263\mathrm{i}$, $I_{1b} = -0.3827 - 0.7618\mathrm{i}$, $I_{1c} = -0.0149 - 0.8277\mathrm{i}$ and $I_{1d} = 0.113 - 4.677\mathrm{i}$.

The behaviour of w_2 for small z has been found by following similar steps.

https://doi.org/10.1017/S0022112004009565 Published online by Cambridge University Press

3.3. *Dispersion relations*

Van Dyke's matching rule has been used on the vertical component of the disturbance velocity to obtain relationships between $B_0(\rho)$, $B_1(\rho)$ and $w_0'(\rho,0)$:

$$H_2\left[w_0(\rho,\epsilon Z)+\epsilon w_1(\rho,\epsilon Z)+\epsilon^2 w_2(\rho,\epsilon Z)\right]=H_2[\epsilon W_0(\rho,z/\epsilon)+\epsilon^2 W_1(\rho,z/\epsilon)], \quad (3.16)$$

where $H_n[\cdot]$ means expand the expression in powers of ϵ retaining terms up to and including $O(\epsilon^n)$. Substituting (3.8*a*, *c*), (3.14) and the corresponding expression for w_2 into (3.16), and eliminating $B_0(\rho)$, $B_1(\rho)$ and $w_0'(\rho,0)$, leads to dispersion relations for ω_1 and ω_2. The result for ω_1 is

$$\omega_1=\frac{\beta_1}{\beta_0}\omega_0-\frac{\rho\alpha_0}{I_{1d}}\left[2\left(\alpha_0\alpha_1+\frac{\beta_0\beta_1}{\rho^2}\right)I_{1a}+\left(\frac{\alpha_1}{\alpha_0}-\frac{\beta_1}{\beta_0}\right)(I_{1b}-I_{1c})+(-\mathrm{i}\omega_0)^{-1/2}\right]. \quad (3.17)$$

The result for ω_2 has also been obtained, but will not be written out here due to its length. However, see the Appendix for the non-parallel part of ω_2.

Before using these dispersion relations to calculate the branch points, we note that there is a relationship between the integrals defined in (3.15) that has an important consequence for the calculation of the non-parallel neutral curve for absolute instability. It follows from a three-dimensional generalization of two-dimensional results presented in appendices of Monkewitz *et al.* (1993). We start by writing the Rayleigh equation (3.10*a*) as $(Q-c_0)(w_0''-\gamma_0^2 w_0)-Q''w_0=0$, which we differentiate with respect to α_0 to give

$$(Q-c_0)\left(\frac{\partial w_0''}{\partial\alpha_0}-\gamma_0^2\frac{\partial w_0}{\partial\alpha_0}\right)-Q''\frac{\partial w_0}{\partial\alpha_0}=2\alpha_0(Q-c_0)w_0+\frac{U''w_0}{\alpha_0}-\frac{UQ''w_0}{\alpha_0(Q-c_0)}+\frac{Q''w_0}{\rho\alpha_0(Q-c_0)}\frac{\partial\omega_0}{\partial\alpha_0}, \quad (3.18)$$

which is a forced Rayleigh equation for $\partial w_0/\partial\alpha_0$. Therefore, multiplying through (3.18) by the solution of the homogeneous adjoint Rayleigh equation, $w_0/(Q-c_0)$, and integrating from 0 to ∞ gives

$$0=\int_0^\infty 2\alpha_0 w_0^2+\frac{U''w_0^2}{\alpha_0(Q-c_0)}-\frac{UQ''w_0^2}{\alpha_0(Q-c_0)^2}+\frac{Q''w_0^2}{\rho\alpha_0(Q-c_0)^2}\frac{\partial\omega_0}{\partial\alpha_0}\,\mathrm{d}z \quad (3.19)$$

and hence, by (3.15),

$$0=2\alpha_0 I_{1a}+\frac{I_{1b}-I_{1c}}{\alpha_0}+\frac{I_{1d}}{\rho\alpha_0}\frac{\partial\omega_0}{\partial\alpha_0}. \quad (3.20)$$

Following a similar method, but differentiating the Rayleigh equation with respect to β_0 instead, leads to

$$0=\frac{2\beta_0}{\rho}I_{1a}-\frac{\rho(I_{1b}-I_{1c})}{\beta_0}+\frac{I_{1d}}{\alpha_0}\frac{\partial\omega_0}{\partial\beta_0}. \quad (3.21)$$

Making use of (3.20) and (3.21) in (3.17), we obtain

$$\omega_1=\frac{\partial\omega_0}{\partial\alpha_0}\alpha_1+\left(\frac{\partial\omega_0}{\partial\beta_0}+\frac{\omega_0}{\beta_0}\right)\beta_1-\frac{\rho\alpha_0}{I_{1d}}(-\mathrm{i}\omega_0)^{-1/2}. \quad (3.22)$$

The coefficient of α_2 in the corresponding expression for ω_2 is also $\partial\omega_0/\partial\alpha_0$, see the Appendix. The appearance of the (complex) 'group velocity' in these expressions resembles the Gaster transformation, see Gaster (1962), where small changes in

https://doi.org/10.1017/S0022112004009565 Published online by Cambridge University Press

spatial growth rate were related to small changes in temporal growth rate by the group velocity. The additional terms in (3.22) represent three-dimensional and viscous effects.

3.4. *Branch points*

The condition for branch points, for a given β, to the order of accuracy of the expansions (3.1), is

$$0 = \frac{\partial \omega}{\partial \alpha} = \frac{\partial \omega / \partial \alpha_0}{\partial \alpha / \partial \alpha_0} = \left(\frac{\partial \omega_0}{\partial \alpha_0} + \epsilon \frac{\partial \omega_1}{\partial \alpha_0} + \epsilon^2 \frac{\partial \omega_2}{\partial \alpha_0} \right) \left(1 + \epsilon \frac{\partial \alpha_1}{\partial \alpha_0} + \epsilon^2 \frac{\partial \alpha_2}{\partial \alpha_0} \right)^{-1}. \tag{3.23}$$

The value of α_0 is chosen so that $\partial \omega_0 / \partial \alpha_0 = 0$ (i.e. (2.13)), then α_1 is chosen so that $\partial \omega_1 / \partial \alpha_0 = 0$ and α_2 is chosen so that $\partial \omega_2 / \partial \alpha_0 = 0$ etc.

Setting the derivative of (3.22) with respect to α_0 to zero, solving for α_1 and evaluating the result for (2.13) gives

$$\alpha_1 = -\frac{1.215 + 0.003\mathrm{i}}{\rho^{1/2}} + (0.3391 + 0.4295\mathrm{i}) \frac{\beta_1}{\rho}. \tag{3.24}$$

It is not necessary to substitute (3.24) into (3.22) because the coefficient of α_1 in ω_1 is zero at a branch point. Numerical evaluation of (3.22) gives

$$\omega_1 = -(0.2309 + 0.1546\mathrm{i}) \rho^{1/2} - (0.3025 + 0.1580\mathrm{i}) \beta_1. \tag{3.25}$$

Along the neutral curve for absolute instability the frequency at the pinch point is real. Therefore, setting the imaginary part of (3.25) to zero and solving for β_1, then substituting this β_1 into (3.24) and (3.25), gives the following values for the pinch points on the neutral curve for absolute instability:

$$\alpha_1 = -(1.546 + 0.423\mathrm{i}) \rho^{-1/2}, \tag{3.26a}$$

$$\beta_1 = -0.9784 \rho^{1/2}, \tag{3.26b}$$

$$\omega_1 = 0.0650 \rho^{1/2}. \tag{3.26c}$$

The result $\beta_1 < 0$ shows that the effect of viscosity along the upper branch of the absolute-instability neutral curve is stabilizing at high enough Reynolds numbers, in qualitative agreement with the behaviour seen for the numerical solutions of the stability equations presented in figure 1, where the neutral curve is apparently approaching the invisicid value from below.

3.5. *Dependence of non-parallel results on choice of measurement quantity*

Before presenting the results for α_2, β_2 and ω_2, it is necessary first to discuss the importance of specifying a measurement quantity when calculating wavenumbers in a non-parallel flow. This is apparent from the factorization of the disturbance in the WKB formulation (2.11) into a slowly varying eigenfunction part and a quickly varying wavy part. Measuring spatial growth rate in an experiment (physical or numerical) requires measuring the disturbance at two near-by values of ρ. The measured change in amplitude will contain a contribution from $\mathrm{Im}(\alpha)$, and from the dependence of the eigenfunction on ρ. This latter term depends on the quantity measured. For example, $u \neq v$ and so the growth rate based on measuring the radial velocity component at some point in the flow will in general be different from the growth rate based on measuring the azimuthal velocity component at the same point (or at a different point, or if some integral measure had been used instead). This property of non-parallel flows means that a variety of neutral curves can be obtained by considering different measurement quantities, see Gaster (1974) for the calculation

https://doi.org/10.1017/S0022112004009565 Published online by Cambridge University Press

of several neutral curves for the Blasius boundary layer. There is no 'right' or 'wrong' choice of measurement quantity, one must simply specify which has been chosen.

The influence of measurement quantity extends to the real part of the wavenumber as well. Let $\hat{q}$ be some measured quantity, i.e. some function of $\hat{u}$, $\hat{v}$, $\hat{w}$ and $\hat{p}$, and so by (2.11) $\hat{q}$ has the form

$$\hat{q} = q(\rho, z) \exp \mathrm{i}Re \left(\int \alpha(\rho)\, \mathrm{d}\rho + \beta\theta - \omega t \right). \tag{3.27}$$

Therefore, the fractional rate of change of $\hat{q}$ in the radial direction is

$$\frac{1}{\hat{q}} \frac{\partial \hat{q}}{\partial \rho} = \frac{\partial \ln \hat{q}}{\partial \rho} = \frac{\partial \ln q}{\partial \rho} + \mathrm{i}Re\, \alpha = \frac{\mathrm{i}\alpha_0}{\epsilon^2} + \frac{\mathrm{i}\alpha_1}{\epsilon} + \mathrm{i}\alpha_2 + \frac{\partial \ln q}{\partial \rho} + O(\epsilon). \tag{3.28}$$

The appearance of α_2 and the measurement term at the same order indicates that the wavy evolution at this order is on the same length scale that the basic flow evolves on. When there is only one evolution length scale, the separation into wavy and non-wavy parts is meaningless. In principle, α_2 could be set to zero (the choice that would be made in an experiment), set to any other value, or absorbed into the measurement term, e.g. by introducing a new measurement function such that $q \to q\mathrm{e}^{-\mathrm{i}\alpha_2 \rho}$. However, we shall write the effective non-parallel wavenumber, based on $\hat{q}$, as

$$\alpha_q = \frac{1}{\mathrm{i}Re} \frac{\partial \ln \hat{q}}{\partial \rho} = \alpha_0 + \epsilon\alpha_1 + \epsilon^2 \left(\alpha_2 - \mathrm{i} \frac{\partial \ln q}{\partial \rho} \right) + O(\epsilon^3). \tag{3.29}$$

The continued explicit presence of α_2 in (3.29) serves to emphasize the arbitrary nature of the wavenumber at $O(Re^{-1})$ in a non-parallel stability calculation, and indicates that for some choices of measurement quantity the range of positions for the neutral curve could be relatively large at finite values of the Reynolds number, since there is no bound on α_2. In a study of convective instability, the neutral curve (for real frequencies) is found by solving $\mathrm{Im}(\alpha_q) = 0$, which depends on the choice made for $\hat{q}$. In a study of absolute instability, the pinch points are located by searching for $\partial\omega/\partial\alpha_q = 0$, which also depends on the choice made for $\hat{q}$.

However, for absolute instability, the potential of there being different neutral curves depending on choice of measurement quantity is problematic. For example, if one choice of disturbance measurement is found to grow in time, but another decays in time, then what happens to the disturbance? If it distorts to accommodate the simultaneous growth and decay of its different characteristics, then its eigenfunction would be changing shape, and the disturbance would no longer be an eigensolution, thus violating the assumption upon which the calculation was based.

The resolution of this potential paradox lies in the manipulations used to derive (3.22) from (3.17), which when applied to the expression for ω_2 show that the coefficient of α_2, and therefore of $\partial \ln q/\partial\rho$ too, is $\partial\omega_0/\partial\alpha_0$, see the Appendix. The determination of the position of the neutral curve in the (Re, β)-plane is therefore independent of the choice of measurement quantity since the coefficient of terms that involve the measurement quantity is zero at a branch point. This conclusion is general and does not only apply to the rotating disk: the neutral curve for absolute instability is unique and does not depend on the choice of measurement quantity, but for waves with non-zero group veocity there will be a range of neutral curves depending on the choice of measurement quantity.

https://doi.org/10.1017/S0022112004009565 Published online by Cambridge University Press

Following the same steps that were used to calculate (3.26), we obtain

$$\alpha_{q2} = \left(-7.11 + 4.19\mathrm{i} - \mathrm{i}\frac{\partial \ln q}{\partial \rho}\right)\frac{1}{\rho}, \tag{3.30a}$$

$$\beta_2 = -4.37, \tag{3.30b}$$

$$\omega_2 = 0.694, \tag{3.30c}$$

where α_{q2} is the $O(\epsilon^2)$ part of α_q. Note that while the evaluation of (3.26) involved the evaluation of integrals of w_0 given in (3.15), (3.30) required the evaluation of integrals involving w_0 and w_1. The w_1 solution was defined in terms of double integrals in (3.13) (to facilitate matching with the viscous solution), but for the numerical evaluation of integrals involving w_1, numerical solutions of (3.10b) were used instead.

In order to determine the contribution made by the non-parallel terms, the calculations in this section have been repeated for the parallel version of the stability equations, i.e. (2.12) with all derivatives with respect to ρ set to zero. The inclusion of α_2 is now essential, and of course the term based on the measurement quantity in (3.29) is now zero. The result is

$$\alpha_2 = -(6.26 - 4.10\mathrm{i})\rho^{-1}, \tag{3.31a}$$

$$\beta_2 = -5.56, \tag{3.31b}$$

$$\omega_2 = 1.15. \tag{3.31c}$$

By comparing (3.30b) with (3.31b), it is clear that the neutral curve for absolute instability predicted by the non-parallel theory lies above that predicted by the parallel theory, and that therefore non-parallel terms are destabilizing, making up about 30% of the $O(Re^{-1})$ contribution to the absolute-instability neutral curve.

4. Comparison between asymptotic and numerical solutions

The predicited destabilization produced by the non-parallel terms represents the leading-order non-parallel effect as $Re \to \infty$. The ability of an asymptotic theory to make accurate quantitative predictions at a given finite Reynolds number depends on the convergence of the series at the given Reynolds number. Many more than the three terms used in (3.1) would be needed before the radius of convergence of the series could be reliably estimated. Instead, the convergence of the asymptotic solution has been tested by comparing it with numerical solutions of the parallelized stability equations. Working in terms of local variables (i.e. taking $\rho = 1$), (2.13b), (3.26b), (3.30b) and (3.31b) give

$$\beta = 0.2652 - 0.9784Re^{-1/2} - 4.37Re^{-1} + O(Re^{-3/2}), \tag{4.1a}$$

$$\beta_p = 0.2652 - 0.9784Re^{-1/2} - 5.56Re^{-1} + O(Re^{-3/2}), \tag{4.1b}$$

for the upper branch of the neutral curve for absolute instability, where the subscript p denotes the parallel-flow result. The asymptotic results (4.1) are shown in figure 2(a) together with the numerical results from figure 1.

What is most striking is how poorly the asymptotic results agree with the numerical results at these Reynolds numbers. It would be expected that the numerical results and asymptotic results would come into closer agreement at higher Reynolds numbers, but figure 2(b) shows that this is not the case. Furthermore, the upper branch of the neutral curve obtained from the numerical solution does not even approach the inviscid result (at least for $Re < 20\,000$), but decays, presumably as some inverse power of Re. As they stand, these results are open to two interpretations: either the

https://doi.org/10.1017/S0022112004009565 Published online by Cambridge University Press

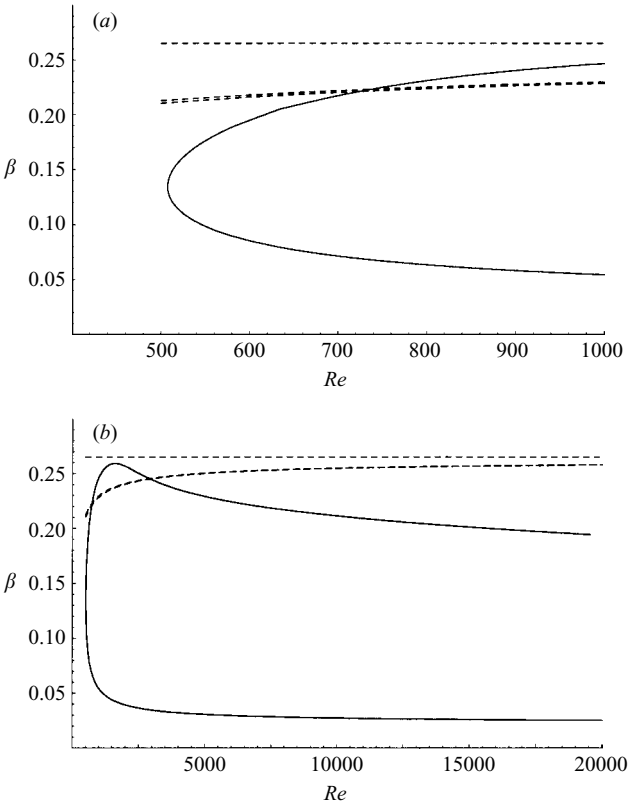


FIGURE 2. (*a*) Solid line is the neutral curve for absolute instability calculated using the sixth-order parallel-flow approximation; top dashed line is the neutral inviscid value (2.13*b*) for absolute instability, middle dashed line is the non-parallel result (4.1*a*), lowest dashed line is the parallel result (4.1*b*). (*b*) Same curves as in (*a*), but plotted over a greater Reynolds number range.

numerical solution has become unreliable at these large-Reynolds-numbers, or the family of branch points discovered by Lingwood (1995) is not the viscous continuation of the inviscid branch points, but is fundamentally of a viscous long-wave character.

This question has been resolved by evaluating (4.1*b*), and the corresponding asymptotic results for α and ω for the branch points, at $Re = 20\,000$, and using these values as initial guesses in the numerical solution procedure for locating branch points with real frequencies. The numerical solution converged quickly to find a second family of branch points extremely close to the asymptotic branch points. This second family of numerically determined branch points is shown in figure 3. The close agreement between the asymptotic theory for the branch points, and the numerical solutions confirms that the numerical solutions are reliable at these Reynolds numbers.

In figure 3 there are two points where the curve for the new family of branch points (those that correspond to the asymptotic theory) intersect the curve of Lingwood's branch points. We shall refer below to the intersection at higher Reynolds number as the 'right-intersection', and to the other intersection point as the 'left-intersection'. At these points, branch points occur at the same β, and each with $\mathrm{Im}(\omega) = 0$, but with different $\mathrm{Re}(\omega)$ and α. In fact, the branch points connect three spatial branches (families of roots of the dispersion relation in the complex α-plane generated by

https://doi.org/10.1017/S0022112004009565 Published online by Cambridge University Press

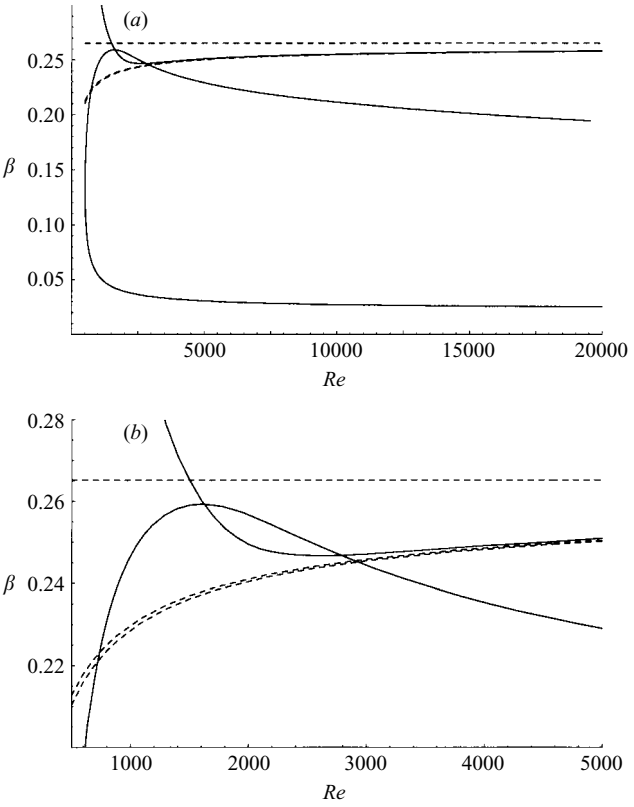


FIGURE 3. Same neutral curves for absolute instability as figure 2, but with an additional family of numerically computed branch points with real frequencies for the sixth-order parallel-flow approximation; (*b*) is a detail of (*a*).

horizontal paths in the ω-plane). One spatial branch lies in the lower half of the complex α-plane for large positive Im(ω), and so is an upstream propagating wave, the other two lie in the upper half of the complex α-plane for large positive Im(ω), and so are downstream propagating waves.

At any given Reynolds number, at most only one of the two families of branch points can give pinch points. Examples of spatial branches close to branch points are shown in figure 4. Figure 4(*a*) is on the neutral curve for the new family of branch points just to the right of the right-intersection point. At this point the new branch point is a pinch point, and Lingwood's branch point is not. Moving to a lower Reynolds number, in between the two intersection points and to a point on Lingwood's family of branch points, figure 4(*b*) shows that here it is Lingwood's branch point that is the pinch point instead. Figure 4(*c*) is on the new family of branch points and to the left of the left-intersection point. Here the branch point is non-pinching and is between two downstream propagating waves.

Thus, all three branches can connect among each other in different combinations and in different orders in this region of parameter space. In fact, this behaviour is controlled by a super branch point where all three branches connect simultaneously. The super branch point is determined by the condition

$$\frac{\partial \omega}{\partial \alpha} = \frac{\partial^2 \omega}{\partial \alpha^2} = 0 \tag{4.2}$$

https://doi.org/10.1017/S0022112004009565 Published online by Cambridge University Press

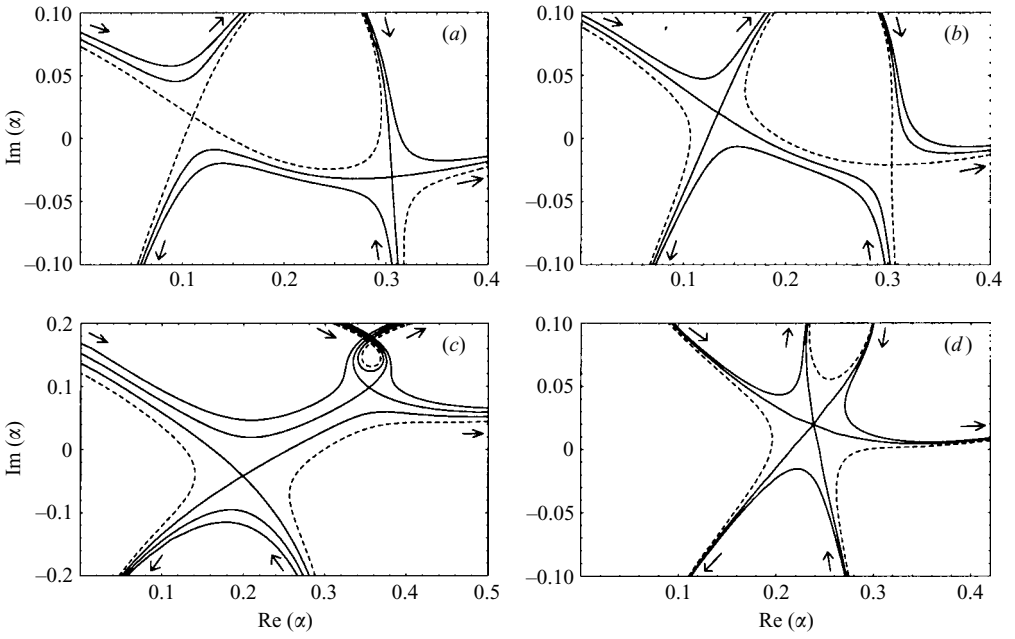


FIGURE 4. Spatial branches, with arrows indicating the direction of increasing Re(ω). In each graph, the spatial branch corresponding to the lowest Im(ω) is represented by a dashed line, and since these are contours below those at the pinch point, they connect the upper-half-plane discreet spectrum to the lower-half-plane discreet spectrum and lie in the valleys of the saddle points. The parameter values used to produce these graphs are (*a*) $Re = 3000$, $\beta = 0.2471$, $\mathrm{Im}(\omega) = 0.00017, 0.000003, -0.000164$, with branch points at $(\alpha, \omega) = (0.1104 + 0.0175\mathrm{i}, -0.06420 - 0.000164\mathrm{i})$ and $(0.3060 - 0.0359\mathrm{i}, -0.06810 + 0.000003\mathrm{i})$; (*b*) $Re = 2600$, $\beta = 0.2467$, $\mathrm{Im}(\omega) = 0.0003, 0.000155, 0.000006$, with branch points at $(\alpha, \omega) = (0.1339 + 0.0203\mathrm{i}, -0.06569 + 0.000155\mathrm{i})$ and $(0.3035 - 0.0208\mathrm{i}, -0.06814 + 0.000006\mathrm{i})$; (*c*) $Re = 1500$, $\beta = 0.265$, $\mathrm{Im}(\omega) = 0.0005, 0.000008, -0.000482, -0.001$, with branch points at $(\alpha, \omega) = (0.1991 - 0.0419\mathrm{i}, -0.07644 - 0.000482\mathrm{i})$ and $(0.3537 + 0.0981\mathrm{i}, -0.07335 + 0.000008\mathrm{i})$; (*d*) $Re = 1994.9$, $\beta = 0.2348$, $\mathrm{Im}(\omega) = 0.0019, 0.00186, 0.0018$.

which we find to occur for $R = 1995$, $\alpha = 0.2385 + 0.0197\mathrm{i}$, $\beta = 0.2348$ and $\omega = -0.06501 + 0.00186\mathrm{i}$. Figure 4(*d*) shows the arrangement of spatial branches close to the super branch point. Note that the usual large-time steepest-descent approximation to the solution of the corresponding initial-value problem (formulated using Fourier-Laplace transforms) breaks down in the case of the super-branch point. This is because these results have the second derivative evaluated at the saddle point appearing in the denominator, and this is zero by (4.2). Nonetheless, a uniformly asymptotic expansion for this case of coalescing saddle points can be constructed in terms of Airy functions, as shown by Chester, Friedman & Ursell (1957).

Figure 5 shows where the super branch point lies in relation to the neutral curves for the two families of branch points, and indicates where each family of branch points produce pinch points. Lingwood's branch points are pinch points near the critical Reynolds number for absolute instability, and along the lower branch of the neutral curve for absolute instability, but only along the upper branch up to $Re = 2790$. For $Re > 2790$ the new family of branch points form the pinch points, and these approach the inviscid results, as the Reynolds number increases, in close agreement with the asymptotic theory developed in § 3. Lingwood's branch points are therefore

https://doi.org/10.1017/S0022112004009565 Published online by Cambridge University Press

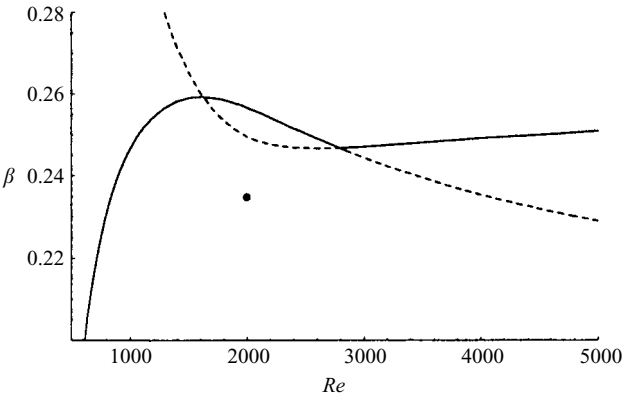


FIGURE 5. Solid lines are the neutral curves for absolute instability, dashed lines are non-pinching branch points with real frequencies, both calculated using the sixth-order parallel-flow approximation. The black dot indicates the position of the super branch point defined by (4.2).

not directly connected to the absolute instability in the inviscid limit, but are related to a long-wave viscous mechanism.

5. Conclusions

A large-Reynolds-number asymptotic theory has been developed to investigate the effect of non-parallel terms on the absolute instability discovered by Lingwood (1995) in the rotating-disk boundary layer. The theory was based on the wavenumber for neutral inviscid absolute instability. It was found that the non-parallel terms have a destabilizing effect on the upper branch of the neutral curve for absolute instability.

Another finding is that although the position of the neutral curve for convective instability depends on the choice of measurement quantity, it has been shown that for absolute instability there is no dependence on the choice of measurement quantity. This is because the term in the dispersion relation that arises from the measurement quantity is multiplied by the complex group velocity, which is zero at the pinch point that produces the absolute instability.

However, a comparison between the asymptotic and numerical solutions for the neutral curve for absolute instability reveals surprisingly poor quantitative agreement. Furthermore, the attempt to improve the agreement by extending the numerical solution to higher Reynolds numbers actually reveals a divergence between the numerical viscous solution and the inviscid solution, which persists, and becomes increasingly exagerated, right up to $Re = 20\,000$, the highest value computed. There might have been concerns that the numerical solution's divergence from the inviscid solution was evidence that it was becoming inaccurate at these large Reynolds numbers. However, taking values from the asymptotic theory as first guesses for branch points in the numerical solution procedure, led to the discovery of a second family of branch points in good agreement with the asymptotic theory. The relation between the two families of branch points, and the regimes where each represent pinch points has been determined. A super branch point has been found where three spatial branches connect simultaneously. Lingwood's branch points are pinch points along the lower branch of the neutral curve for absolute instability, around the critical Reynolds number for absolute instability, but only up to $Re = 2790$ on the upper

https://doi.org/10.1017/S0022112004009565 Published online by Cambridge University Press

branch. The new family of branch points form pinch points for $Re > 2790$, and it is this second family that connects to the inviscid results.

This discovery of the second family of pinch points does not have direct practical consequences, because the flow is always likely to be turbulent at the Reynolds numbers where the new family becomes important. Its significance lies in clarifying the relationship between the viscous and inviscid theories of absolute instability on the rotating disk. The stationary vortices in the rotating-disk boundary layer were discovered first in the inviscid theory, and later found in the viscous theory. The simple connection known to exist between the viscous and inviscid stationary vortices allows the inviscid theory to be used as a starting point for nonlinear investigations. It also determines the order of magnitude of non-parallel effects since it fixes the ratio between vortex wavelength and basic flow evolution, and so helps justify use of the parallel-flow approximation in studies of stationary vortices.

When Lingwood (1995) found absolute instability in both the viscous and inviscid theories, she assumed that a correspondingly simple relation existed between the two, and argued that, therefore, non-parallel effects would be as small for the absolute instability as they are for stationary vortices. However, the results presented here show that this is not the case. Instead, Lingwood's family of branch points is controlled by a long-wave viscous mechanism. This means that non-parallel effects will be larger by some power of the Reynolds number than previously assumed. It also shows that the inviscid theory with order unity eigenvalues is not an appropriate starting point for modelling absolute instability in the rotating-disk boundary layer.

A complete theoretical understanding of this local absolute instability lies in the viscous long-wave limit. Such a theory can be developed from the inviscid long-wave theory of Healey (2004), which includes the fundamental instability mechanism itself, and shows that in this limit there are several families of branch points, only one of which is pinching, with two downstream propagating modes and a single upstream propagating mode, thus reproducing all the main characteristics of the dispersion relation discovered here at finite Reynolds numbers. The viscous long-wave theory for the absolute instability will inherit these characteristics of the inviscid long-wave theory, and the addition of viscous terms will allow the Reynolds number scalings, and asymptotic disturbance structure, of the lower branch of the neutral curve to be determined as well.

Finally, we point out that the destabilizing effect of non-parallel terms on the local absolute-instability characteristics found here does not contradict the stabilizing effect of spatial inhomogeneity found in the direct numerical simulations of disturbances in the rotating-disk boundary layer by Davies & Carpenter (2003). As described in the introduction, the global behaviour can be stable even when there is local absolute instability. The linear global behaviour is nonetheless determined by the local stability characteristics, and the methods presented here for carrying out non-parallel local calculations could in principle be used to develop linear and nonlinear global-mode theories for the rotating-disk boundary layer.

Appendix. The non-parallel terms in the asymptotic theory

The non-parallel terms enter the expansions at $O(Re^{-1}) = O(\epsilon^2)$ and so modify the α_2, β_2 and ω_2 terms in (3.1). The Coriolis and streamline curvature terms also enter at this order, and the viscous terms enter in the main part of the boundary layer. Consequently, the expressions for the dispersion relation, and hence branch points, at this order contain very many terms, and so will not be written out here fully.

https://doi.org/10.1017/S0022112004009565 Published online by Cambridge University Press

Nonetheless, the terms of most interest to us are the non-parallel terms, and these can be extracted from the result for ω_2:

$$\omega_2 = \omega_{2\mathrm{p}} + \left(\alpha_{2\mathrm{n}} - \mathrm{i}\frac{\partial \ln q}{\partial \rho}\right)\frac{\partial \omega_0}{\partial \alpha_0} + \beta_{2\mathrm{n}}\left(\frac{\partial \omega_0}{\partial \beta_0} + \frac{\omega_0}{\beta_0}\right) - \mathrm{i}\frac{\beta_0^2}{\rho^3\gamma_0^4}\left(\gamma_0^2 + 2\alpha_0^2\right)$$
$$\times\left(\frac{\partial \omega_0}{\partial \alpha_0} - \frac{\rho^2\alpha_0}{\beta_0}\frac{\partial \omega_0}{\partial \beta_0}\right) + 2\mathrm{i}\frac{c_0\alpha_0^2}{\rho\gamma_0^2} + \frac{\mathrm{i}}{I_{1d}}\left[\alpha_0^2 I_{2a} + \left(\frac{\beta_0}{\rho}\right)^2 I_{2b} - \frac{c_0\alpha_0^2}{\rho\gamma_0^2}(I_{2c} - I_{2d})\right.$$
$$\left. + \left(\frac{\alpha_0}{\gamma_0}\right)^2 (I_{2e} + I_{2f} - I_{2g} + I_{2h}) + I_{2f} + I_{2i} - I_{2j} - I_{2k} + I_{2l} + I_{2m} + I_{2n} - I_{2o}\right] \tag{A1}$$

where

$$I_{2a} = \frac{1}{w_0'(\rho,0)^2}\int_0^\infty \frac{Qw_0^2}{Q-c_0}\,\mathrm{d}z, \qquad I_{2b} = \frac{1}{w_0'(\rho,0)^2}\int_0^\infty \frac{Uw_0^2}{Q-c_0}\,\mathrm{d}z, \tag{A2a,b}$$

$$I_{2c} = \frac{1}{w_0'(\rho,0)^2}\int_0^\infty \frac{(Q')^2w_0^2}{(Q-c_0)^3}\,\mathrm{d}z, \quad I_{2d} = \frac{1}{w_0'(\rho,0)^2}\int_0^\infty \frac{Q'w_0w_0'}{(Q-c_0)^2}\,\mathrm{d}z, \tag{A2c,d}$$

$$I_{2e} = \frac{1}{w_0'(\rho,0)^2}\int_0^\infty \frac{U(Q')^2w_0^2}{(Q-c_0)^3}\,\mathrm{d}z, \quad I_{2f} = \frac{1}{w_0'(\rho,0)^2}\int_0^\infty \frac{U'Q'w_0^2}{(Q-c_0)^2}\,\mathrm{d}z, \tag{A2e,f}$$

$$I_{2g} = \frac{1}{w_0'(\rho,0)^2}\int_0^\infty \frac{UQ'w_0w_0'}{(Q-c_0)^2}\,\mathrm{d}z, \quad I_{2h} = \frac{1}{w_0'(\rho,0)^2}\int_0^\infty \frac{U'w_0w_0'}{Q-c_0}\,\mathrm{d}z, \tag{A2g,h}$$

$$I_{2i} = \frac{1}{w_0'(\rho,0)^2}\int_0^\infty \frac{(U')^2w_0^2}{(Q-c_0)^2}\,\mathrm{d}z, \quad I_{2j} = \frac{1}{w_0'(\rho,0)^2}\int_0^\infty \frac{U''Qw_0^2}{(Q-c_0)^2}\,\mathrm{d}z, \tag{A2i,j}$$

$$I_{2k} = \frac{1}{w_0'(\rho,0)^2}\int_0^\infty \frac{U'Qw_0w_0'}{(Q-c_0)^2}\,\mathrm{d}z, \quad I_{2l} = \frac{1}{w_0'(\rho,0)^2}\int_0^\infty \frac{UU'w_0w_0'}{(Q-c_0)^2}\,\mathrm{d}z, \tag{A2k,l}$$

$$I_{2m} = \frac{1}{w_0'(\rho,0)^2}\int_0^\infty \frac{U^2Q''w_0^2}{(Q-c_0)^3}\,\mathrm{d}z, \quad I_{2n} = \frac{1}{w_0'(\rho,0)^2}\int_0^\infty \frac{U'QQ'w_0^2}{(Q-c_0)^3}\,\mathrm{d}z, \tag{A2m,n}$$

$$I_{2o} = \frac{1}{w_0'(\rho,0)^2}\int_0^\infty \frac{UU'Q'w_0^2}{(Q-c_0)^3}\,\mathrm{d}z, \tag{A2o}$$

and $\omega_{2\mathrm{p}}$ represents all the terms that would be present in an analysis of the parallel-flow equations, $\alpha_{2\mathrm{n}}$ and $\beta_{2\mathrm{n}}$ are the non-parallel corrections to the wavenumbers and q is some measurement quantity as discussed in § 3.5. The derivative $\partial\omega_2/\partial\alpha_0$ is then calculated and set to zero to solve for α_2 at the pinch point, then setting the imaginary part of ω_2 to zero and solving for $\beta_{2\mathrm{n}}$ leads to the non-parallel contribution to the pinch point giving the upper branch of the neutral curve of absolute instability.

REFERENCES

Batchelor, G. K. 1951 Note on a class of solutions of the Navier–Stokes equations representing steady rotationally-symmetric flow. *Q. J. Mech. Appl. Maths* **4**, 29–41.

Batchelor, G. K. 1967 *An Introduction to Fluid Dynamics*. Cambridge University Press.

Benton, E. R. 1966 On the flow due to a rotating disk. *J. Fluid Mech.* **24**, 781–800.

Bertolotti, F. P., Herbert, T. & Spalart, P. R. 1992 Linear and nonlinear stability of the Blasius boundary layer. *J. Fluid Mech.* **242**, 441–474.

Bödewadt, U. T. 1940 Die Drehströmung über festem Grunde. *Z. Angew. Math. Mech.* **20**, 241–253.

Briggs, R. J. 1964 *Electron-Stream Interaction with Plasmas*. MIT Press.

https://doi.org/10.1017/S0022112004009565 Published online by Cambridge University Press

Chester, C., Friedman, B. & Ursell, F. 1957 An extension of the method of steepest descents. *Proc. Camb. Phil. Soc.* **53**, 599–611.

Davies, C. & Carpenter, P. W. 2003 Global behaviour corresponding to the absolute instability of the rotating-disk boundary layer. *J. Fluid Mech.* **486**, 287–239.

Ekman, V. W. 1905 On the influence of the earth's rotation on ocean currents. *Ark. Mat. Astr. Fys.* **2** No. 11.

Gaster, M. 1962 A note on the relation between temporally-increasing and spatially-increasing disturbances in hydrodynamic stability. *J. Fluid Mech.* **14**, 222–224.

Gaster, M. 1974 On the effects of boundary layer growth on flow stability. *J. Fluid Mech.* **66**, 465–480.

Gregory, N., Stuart, J. T. & Walker, W. S. 1955 On the stability of three-dimensional boundary layers with application to the flow due to a rotating disk. *Phil. Trans. R. Soc. Lond.* A **248**, 155–199.

Hall, P. 1983 The linear development of Görtler vortices in boundary layers. *J. Fluid Mech.* **130**, 41–58.

Hall, P. 1986 An asymptotic investigation of the stationary modes of instability of the boundary layer on a rotating disk. *Proc. R. Soc. Lond.* A **406**, 93–106.

Healey, J. J. 2004 Inviscid long-wave theory for the absolute instability of the rotating-disk boundary-layer. *J. Fluid Mech.* (Submitted).

Huerre, P. 2000 Open shear flow instabilities. In *Perspectives in Fluid Dynamics* (ed. G. K. Batchelor, H. K. Moffatt & M. G. Worster), pp. 159–229. Springer.

Huerre, P. & Monkewitz, P. A. 1990 Local and global instabilities in spatially developing flows. *Annu. Rev. Fluid Mech.* **22**, 473–537.

von Kármán, Th. 1921 Über laminare und turbulente Reibung. *Z. Angew. Math. Mech.* **1**, 233–252.

Kuiken, H. K. 1971 The effect of normal blowing on the flow near a rotating disk of infinite extent. *J. Fluid Mech.* **47**, 789–798.

Lingwood, R. J. 1995 Absolute instability of the boundary layer on a rotating disk. *J. Fluid Mech.* **299**, 17–33.

Lingwood, R. J. 1997 Absolute instability of the Ekman layer and related rotating flows. *J. Fluid Mech.* **331**, 405–428.

Monkewitz, P. A., Huerre, P. & Chomaz, J.-M. 1993 Global linear stability analysis of weakly non-parallel shear flows. *J. Fluid Mech.* **251**, 1–20.

Orszag, S. A. 1971 Accurate solution of the Orr–Somerfeld stability equation. *J. Fluid Mech.* **50**, 689–703.

Pier, B. 2003 Finite-amplitude crossflow vortices, secondary instability and transition in the rotating-disk boundary layer. *J. Fluid Mech.* **487**, 315–343.

Smith, F. T. 1979 On the non-parallel flow stability of the Blasius boundary layer. *Proc. R. Soc. Lond.* A **366**, 91–109.

Soward, A. M. & Jones, C. A. 1983 The linear stability of the flow in the narrow gap between two concentric rotating spheres. *Q. J. Mech. Appl. Maths* **36**, 19–42.

Stuart, J. T. 1954 On the effects of uniform suction on the steady flow due to a rotating disk. *Q. J. Mech. Appl. Maths* **7**, 446–457.

https://doi.org/10.1017/S0022112004009565 Published online by Cambridge University Press